July 1980

Theoretical potential curves for excited states of ArH and the rate of collisional quenching of metastable Ar by H

R.L. Vance
University of Nebraska - Lincoln

Gordon A. Gallup
UNL, ggallup1@unl.edu

Theoretical potential curves for excited states of ArH and the rate of collisional quenching of metastable Ar by H[a)]

R. L. Vance and G. A. Gallup

Department of Chemistry, University of Nebraska, Lincoln, Nebraska 68588
(Received 2 March 1979; accepted 16 January 1980)

Energy curves for the ground state and the first seven excited states of ArH have been calculated using the multiconfiguration valence bond (MCVB) method. Important features of the excited curves include two distinct avoided crossings between the lowest Ar*H and the highest ArH* potential energy curves. Using these curves we have made a theoretical analysis of quenching of metastable Ar by collision with H at room temperature. Application of the Massey criterion indicates that the separation of the potential curves in the region of the crossing and the acceleration produced by the fall of the reactant channel potential curve from its asymptotic level combine to produce a relatively high probability for curve switching. A more quantitative estimate of the curve switching probability is given with the Landau–Zener formula and leads to a theoretical value of the quenching rate approximately ten times the experimental. In light of the many approximations involved this qualitative agreement is satisfactory and provides a rationale to explain the anomalously high rate constant for the quenching reaction. Structural features of the interacting potential curves are discussed in terms of the diabatic states involved.

I. INTRODUCTION

The theoretical understanding of energy transfer reactions involving metastable states of rare-gas atoms are of great scientific interest, as well as being important in the practical design of rare-gas–halide lasers. The collisional quenching of metastable Ar atoms by H atoms is a simple example of energy transfer and is an excellent prototypical system for theoretical study. In addition, during the past few years experimental results on the Ar–H system have been accumulating, and the interpretation of these results will be greatly aided by having reliable theoretical energy curves. In this article we report on an *ab initio* calculation of the seven lowest lying energy curves for Ar–H. We use these results to give an estimate of the second-order rate constant for quenching of metastable Ar by H-atom collision. We also include a discussion of the conclusions possible concerning the diabatic states involved.

Johns[1] reported the first gas phase emission spectrum of neutral argon hydride near 7060 Å. The spectrum was identified as being due to an ArH transition between two excited electronic states of $^2\Sigma^+$ and $^2\Pi$ symmetry. Similar spectra are not observed for helium or neon hydrides.

Bondybey *et al.*,[2] in their study of the matrix isolation of H_2Br in argon, observed a sharp infrared absorption at 644 cm^{-1}. At the time the absorption was attributed to a reactive impurity and therefore ignored in their discussion of H_2Br. However, Bondybey and Pimentel[3] demonstrated in later experiments that the 644 cm^{-1} absorption is present in the absence of the halogen, that is, with only the argon matrix and deuterium. They concluded that the absorption is due to isolated H atoms trapped in O_h interstitial sites in solid argon. Their interpretation was later supported by *ab initio* calculations for H atoms trapped in a neon lattice.[4]

Even more recently, Setser and co-workers[5] have measured the room temperature rate constant for quenching of $Ar(^3P)$ by ground state H atoms.

$$Ar^*(^3P) + H(1s) \rightarrow Ar + H^*(2s, 2p) . \quad (1)$$

$Ar(^3P)$ atoms have 11.54 eV of available energy, and since only 10.2 eV of this energy is needed to excite the H ($2s$ and $2p$) level, reaction (1) has a large energy defect of 1.3 eV. The measured rate constant, 2.4×10^{-10} cm^3/sec is surprisingly large for a process with a single exit channel and an energy defect of this magnitude. They discuss the H atom excitation in terms of a double curve crossing mechanism. We shall return to this question later and compare their description of the process to our calculations.

Numerous theoretical calculations have been made of the ground state of argon hydride.[6] However, theoretical studies for low-lying excited states have been sparse. Recently, Matcha and Milleur[7] have reported the results of linear combination of atomic orbitals–self-consistent field–molecular orbitals (LCAO-SCF-MO) calculations for ground state ArH and the excited states of $ArH^*(n=2)$. Also, Olson and Liu[8] have made SCF–configuration interaction (CI) calculations for ground state ArH and the excited states of $ArH^*(n=2)$. However, there have been no reported theoretical calculations including the excited states of $Ar^*(n=4)$ H.

In our studies we have directed our attention to the *ab initio* calculation of the potential curves needed to analyze the excitation transfer between excited ^{3}Ar and H. The multiconfiguration valence bond (MCVB) method has been used to obtain adiabatic potential curves for the ground state and first seven excited states. These provide the necessary energy parameters for an estimation of the rate constant for reaction (1) by the familiar Landau–Zener formula.[9] Comparisons with previous calculations will be made where possible.

[a)] Based in part upon the thesis submitted by R. L. Vance to the Graduate Faculty in the University of Nebraska in partial fulfillment of the requirements for the Ph.D. degree.

 0021-9606/80/140894-08$01.00

II. POTENTIAL CURVES

All calculations have been done with the multiconfigurational valence bond method.[10] We neglect magnetic effects in the Hamiltonian and use the Born–Oppenheimer approximation to obtain the adiabatic energy curves. The wave functions for a desired electronic state are expanded in terms of an N-particle basis of nonorthogonal tableau symmetry functions (TSF), each TSF being a linear combination of atomic orbital (AO) products.[10]

The AO's used consisted of a $1s$, $2s$, $2p$ set on hydrogen and a $1s$, $2s$, $2p$, $3s$, $3p$, $4s$, $4p$ set on argon. The hydrogen orbitals are those given by Whitten[11] and the $1s-3p$ Ar orbitals are the SCF orbitals in terms of the $[6s, 3p]$ set of Gaussian functions given by Petke *et al.*[12] The above $[6s, 3p]$ set was augmented with a three term $4s$ Gaussian-type orbital (GTO) and a set of three term $4p$ GTO's given by Sramek and Gallup.[13] The $4s$ and $4p$ orbital parameters are given in Table I.

The argon $4s$ and $4p$ atomic orbitals were obtained by first performing a SCF calculation for the Ar atom. The basis set consisted of the $[7s, 4p]$ set described above. From this calculation, the six lowest-energy SCF s-type orbitals (three closed and three virtual) and the four lowest-energy SCF p-type orbitals (two closed and two virtual) were used as the basis set for a limited CI calculation. The Ar: $(1s)^2\ (2s)^2\ (2p)^6\ (3s)^2$ SCF orbitals were frozen in all configurations. The CI wave function was expanded in terms of the ground state SCF configuration and all configurations resulting from a single excitation from the p_y orbital into one of the SCF virtual orbitals. Thus, there was a total of ten configurations.

The CI ground state wavefunction, because of Brillouin's theorem, consisted only of the SCF ground state configuration. The first excited state CI wave function consisted only of configurations resulting from a single excitation of a p_y electron into one of the SCF virtual s-type orbitals,

$$\Psi_{\mathrm{CI}}^{(1)} = \sum_{i=1}^{3} c_i^{(1)} (p_x)^2 (p_x)^2 (p_y)^1 (v_{s_i})^1 , \tag{2}$$

where v_{s_i} represents one of the SCF s-type virtual orbitals. The argon $4s$ atomic orbital is then taken as

$$c_1^{(1)} v_{s_1} + c_2^{(1)} v_{s_2} + c_3^{(1)} v_{s_3} . \tag{3}$$

TABLE I. Argon $4s$ and $4p$ orbital parameters.

Orbital	Coefficient	Scale factor
$4p^a$	0.226 178	0.032 694 9
	0.861 282	0.069 244 0
	−0.178 258	0.564 149
$4s$	0.125 882	0.021 965 6
	1.125 882	0.044 486 1
	−0.334 922	0.226 787

[a] $4p$ functions have lobe separations defined by the relationship $\alpha_i \delta_i^2 = 0.01$, where α_i is the scale factor and δ_i is the lobe separation.

TABLE II. Comparison of the MCVB asymptotic Ar* ($4s$) H energy difference and the experimental difference.

MCVB		Experimental[a]	
State	Energy (eV)	State	Energy (eV)
^{3}Ar* ($4s$) H, $^2\Sigma^+$	11.618	Ar ($4s_1$, $^3p_2$)	11.548
^{3}Ar* ($4s$) H, $^2\Pi$	11.622	Ar ($4s$, $^3p_1$)	11.623
^{1}Ar* ($4s$) H, $^2\Sigma^+$	11.870	Ar ($4s$, $^3p_0$)	11.723
^{1}Ar* ($4s$) H, $^2\Pi$	11.874	Ar ($4s_1$, $^1p_1$)	11.828

[a] Multiplet averages, Ref. 20.

The Ar*($4s$) excited state is now representable by a single TSF

$$\Theta NPN[3p_x(1)\,3p_y(2)\,3p_z(3)\,3p_x(4)\,3p_y(5)\,4s(6)] , \tag{4}$$

where ΘNPN is the Young operator appropriate for the desired multiplicity and $4s = c_1^{(1)} v_{s_1} + c_2^{(1)} v_{s_2} + c_3^{(1)} v_{s_3}$. The argon $4p$ orbital was constructed in a manner completely analogous to the one just described.

In spite of the neglect of spin–orbit effects the above procedure produces good approximations to the energy spacings of the atomic $4s$ and $4p$ excited states of argon. A comparison between our asymptotic *ab initio* Ar*($4s$)H energy differences and experiment is given in Table II. As may be seen, the calculated differences are all within 0.1 eV of the experimental differences, and we have found it unnecessary to adjust the level of our calculated curves to match experiment.

For the molecular calculations, the Ar: $(1s)^2\ (2s)^2 \times (2p)^6\ (3s)^2$ atomic orbitals have been frozen in all TSF's. Keeping the $3s$ orbital doubly occupied is expected to have no serious effects except at close distances where significant amounts of Ar $3s-3p$ hybridization may occur.

The valence bond wave function for states of $^2\Sigma^+$ symmetry include: (1) the TSF's

$$\Theta NPN[3p_z(1)\,3p_x(2)\,3p_y(3)\,\mathrm{H}1s(4)\,3p_z(5) \times 3p_x(6)\,3p_y(7)]$$

and

TABLE III. Dominant molecular states of $^2\Sigma^+$ symmetry.

Molecular states	Tableau symmetry functions
I. ArH	$\Theta NPN[3p_z\,3p_x\,3p_y\,\mathrm{H}1s\,3p_z\,3p_x\,3p_y]$[a]
II. ArH* ($2s$)	$\Theta NPN[3p_z\,3p_x\,3p_y\,\mathrm{H}2s\,3p_z\,3p_x\,3p_y]$
III. ArH* ($2p_\sigma$)	$\Theta NPN[3p_z\,3p_x\,3p_y\,\mathrm{H}2p_z\,3p_z\,3p_x\,3p_y]$
IV. Ar^+ ($^2P_\sigma$) H^-	$\Theta NPN[\mathrm{H}1s\,3p_x\,3p_y\,3p_z\,\mathrm{H}1s\,3p_x\,3p_y]$ $\Theta NPN[3p_x\,3p_y\,\mathrm{H}2s\,3p_z\,3p_x\,3p_y\,\mathrm{H}1s]$
V. Ar^- ($4s\ ^2S$) H^+	$\Theta NPN[3p_x\,3p_y\,3p_z\,4s\,3p_x\,3p_y\,3p_z]$
VI. Ar* ($^3P_\sigma$) H	$\Theta NPN[3p_x\,3p_y\,4p_z\,3p_z\,3p_x\,3p_y\,\mathrm{H}1s]$
VII. Ar* ($^1P_\sigma$) H	$\Theta NPN[3p_x\,3p_y\,4p_z\,3p_z\,3p_x\,3p_y\,\mathrm{H}1s]$ $\Theta NPN[3p_x\,3p_y\,4p_z\,\mathrm{H}1s\,3p_x\,3p_y\,3p_z]$

[a] The particle labels are 1, 2, ..., 7 in the same order as the orbital labels and are implied.

TABLE IV. Dominant molecular states of $^2\Pi$ symmetry.

Molecular states	Tableau symmetry functions
I. $ArH^*(2p_\pi)$	$\Theta NPN[3p_z 3p_y 3p_x H2p_x 3p_z 3p_y 3p_x]$[a]
II. $Ar^+(^2P_\pi)\ H^-$	$\Theta NPN[3p_z 3p_y H1s 3p_x 3p_z 3p_y H1s]$
III. $Ar^+(^2P_\pi)\ H^{-3}\ (1s, 2s)$	$\Theta NPN[3p_z 3p_y H2s H1s 3p_z 3p_y 3p_x]$
IV. $Ar^+(^2P_\sigma)\ H^{-3}\ (1s, 2p_\pi)$	$\Theta NPN[3p_y 3p_x 3p_z H1s 3p_y 3p_x H2p_x]$ $\Theta NPN[3p_y 3p_x 3p_z H2p_x 3p_y 3p_x H1s]$
V. $Ar^+(^2P_\sigma)\ H^{-1}\ (1s, 2p_\pi)$	$\Theta NPN[3p_y 3p_x 3p_z H1s 3p_y 3p_x H2p_x]$ $\Theta NPN[3p_y 3p_x 3p_z H2p_x 3p_y 3p_x H1s]$
VI. $Ar^*(4s,\ ^3P_\pi)\ H$	$\Theta NPN[3p_z 3p_y 4s 3p_x 3p_z 3p_y H1s]$
VII. $Ar^*(4s,\ ^1P_\pi)\ H$	$\Theta NPN[3p_z 3p_y 4s H1s 3p_z 3p_y 3p_x]$ $\Theta NPN[3p_z 3p_y 4s 3p_x 3p_z 3p_y 3p_x]$

[a]See footnote Table III.

$$\Theta NPN[H1s(1)\,3p_x(2)\,3p_y(3)\,3p_z(4)\,H1s(5)\times 3p_x(6)\,3p_y(7)]$$

and (2) all TSF's resulting from single and double excitations into the H2s, H2p_σ, Ar4s, Ar4p_σ, and Ar4p_π atomic orbitals from the above two TSF's. Also, the charge on the hydrogen atomic state cannot be less than -1. The above procedure gives a total of 114 TSF's and produces the necessary functions for the description of all the $^2\Sigma^+$ states under consideration. In Table III we have listed the seven dominant molecular configurations and the nine TSF's necessary for their representation in the MCVB wave function. If we were discussing a system like HCl, these principal configurations could be described in terms of covalent and ionic contributions to the bond. The extra electron in ArH clouds the distinctions between such terms, but each of these configurations contribute significantly both to covalent and ionic type bonding between the two atoms in the excited states considered. Our excitation scheme also produces TSF's which contribute to the description of the molecular and assymptotic atomic states. Similar single and double excitation schemes have been used successfully with other systems to discuss both long-range forces[14] and chemical bonding in hydrogen fluoride.[15]

The MCVB wave function for states of $^2\Pi$ symmetry include: (1) the eight TSF's

$$\Theta NPN[3p_y(1)\,3p_x(2)\,3p_z(3)\,H1s(4)\,3p_y(5)\,3p_x(6)\,H2p_x(7)],$$
$$\Theta NPN[3p_y(1)\,3p_x(2)\,3p_z(3)\,H2p_x(4)\,3p_y(5)\,3p_x(6)\,H1s(7)],$$
$$\Theta NPN[3p_z(1)\,3p_x(2)\,3p_y(3)\,H2p_x(4)\,3p_z(5)\,3p_x(6)\,H2p_y(7)],$$
$$\Theta NPN[3p_z(1)\,3p_x(2)\,3p_y(3)\,H2p_y(4)\,3p_z(5)\,3p_x(6)\,H2p_x(7)],$$
$$\Theta NPN[3p_z(1)\,3p_y(2)\,H1s(3)\,3p_x(4)\,3p_z(5)\,3p_y(6)\,H1s(7)],$$
$$\Theta NPN[3p_z(1)\,3p_y(2)\,H2p_y(3)\,3p_x(4)\,3p_z(5)\,3p_y(6)\,H2p_y(7)],$$
$$\Theta NPN[3p_z(1)\,3p_y(2)\,H2p_x(3)\,3p_x(4)\,3p_z(5)\,3p_y(6)\,H2p_x(7)],$$

and

$$\Theta NPN[3p_z(1)\,3p_y(2)\,3p_x(3)\,H2p_x(4)\,3p_z(5)\,3p_y(6)\,3p_x(7)],$$

and (2) all TSF's resulting from single and double excitations into the H2p_σ, H2s, Ar4s, Ar4p_σ, and Ar4p_π atomic orbitals from the above set of TSF's. Again the wave function is restricted by requiring the hydrogen atomic states in each TSF to have a charge no less than -1. This gives a total of 165 TSF's. The seven dominant molecular configurations and their associated TSF's are given in Table IV. The computed energies for the ArH states are presented in Table V and depicted graphically in Fig. 1. The discussion of configuration selection above for the Σ states applies to these Π states as well.

TABLE V. Interaction potential energies for the eight lowest states of ArH (units are hartrees, 1 h = 27.2107 eV).

$R(a_0)$	$X\,^2\Sigma^+$	$A\,^2\Sigma^+$	$B\,^2\Pi$	$C\,^2\Sigma^+$	$D\,^2\Pi$	$E\,^2\Sigma^+$	$F\,^2\Pi$	$G\,^2\Sigma^+$
1.50	−526.471 39	−526.389 25	−526.397 70	−526.347 09	−526.213 03	−526.317 87	−525.786 32	−525.926 16
1.75	−526.792 69	−526.709 01	−526.714 64	−526.673 80	−526.542 46	−526.635 13	−526.177 49	−526.342 88
2.00	−526.963 73	−526.874 86	−526.873 05	−526.845 83	−526.711 23	−526.785 96	−526.421 04	−526.579 63
2.25	−527.066 25	−526.960 58	−526.948 42	−526.927 84	−526.794 81	−526.850 73	−526.580 83	−526.706 34
2.50	−527.136 59	−526.998 16	−526.979 97	−526.961 46	−526.832 40	−526.870 90	−526.689 15	−526.768 98
2.60	···	−527.004 66	−526.985 41	−526.967 20	···	···	···	···
2.70	···	−527.007 96	−526.988 11	−526.970 07	···	···	···	···
2.75	−527.186 30	−527.008 65	−526.988 65	−526.970 66	−526.845 03	−526.868 62	−526.764 14	−526.797 33
2.80	···	−527.008 83	−526.988 76	−526.970 79	···	···	···	···
2.90	···	−527.007 87	−526.987 86	−526.969 88	···	···	···	···
3.00	−527.221 16	−527.005 59	−526.985 81	−526.967 79	−526.844 72	−526.857 25	−526.816 50	−526.808 81
3.25	−527.245 42	−526.996 31	−526.977 69	−526.959 37	−526.852 99	−526.850 39	−526.837 70	−526.826 21
3.50	−527.262 26	−526.984 78	−526.967 65	−526.948 97	−526.877 76	−526.867 77	−526.828 15	−526.828 59
3.75	−527.273 95	−526.973 15	−526.957 62	−526.938 63	−526.894 19	−526.885 44	−526.821 04	−526.826 82
4.00	−527.282 02	−526.962 54	−526.948 51	−526.929 49	−526.904 60	−526.896 61	−526.831 83	−526.827 66
4.50	−527.291 42	−526.945 97	−526.934 61	−526.918 21	−526.913 65	−526.903 10	−526.845 37	−526.833 62
5.00	−527.295 83	−526.934 85	−526.926 35	−526.915 19	−526.913 73	−526.898 71	−526.852 29	−526.841 89
6.00	−527.298 82	−526.922 54	−526.920 32	−526.909 53	−526.903 89	−526.899 79	−526.858 98	−526.857 41
7.00	−527.299 39	−526.919 71	−526.919 34	−526.906 31	−526.891 94	−526.897 55	−526.862 41	−526.863 14
8.00	−527.299 43	−526.919 27	−526.919 27	−526.911 86	−526.882 51	−526.887 87	−526.864 06	−526.865 42
9.00	−527.299 36	−526.919 17	−526.919 29	−526.915 35	−526.876 85	−526.880 68	−526.864 42	−526.866 00
10.00	−527.299 27	−526.919 14	−526.919 30	−526.917 25	−526.874 20	−526.876 50	−526.864 13	−526.865 56
20.00	−527.299 05	−526.919 31	−526.919 30	−526.918 95	−526.871 95	−526.872 08	−526.862 69	−526.862 81

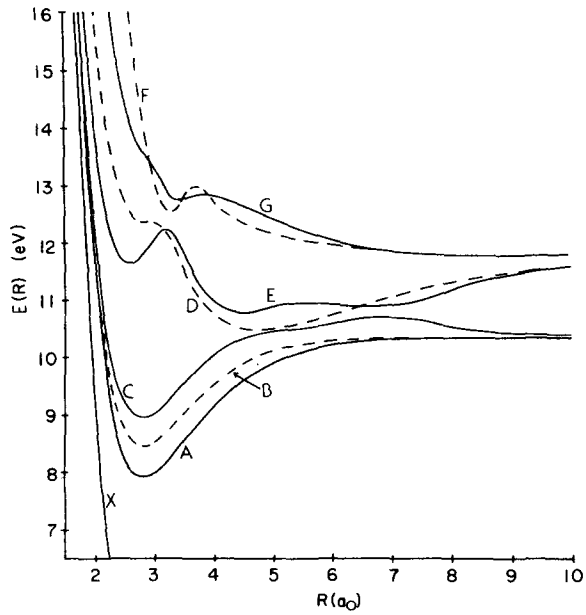

FIG. 1. Potential curves for the first seven excited states of ArH. The zero of energy is taken as the infinitely separated atoms in their ground states. The X, A, C, E, and G states are all $^2\Sigma$. (solid curves). The B, D, and F states are all $^2\Pi$. (Dashed curves.)

The first three excited states of ArH are usually thought of approximately as ArH^+ with an electron in a Rydberg state, and the potential curves for these states should have shapes similar to that of the $ArH^+(X^1\Sigma^+)$ potential. The interatomic potential for this system has been well characterized by Klingbeil.[16] Using elastic differential cross section data, he determined the binding energy to be 4.17 eV and the equilibrium separation to be 2.42 bohrs. Therefore, one would expect the states $A^2\Sigma^+$, $B^2\Pi$, and $C^2\Sigma^+$ to have equilibrium bond lengths of approximately 2.42 bohrs. This expectation is in agreement with the experimental work of Johns,[1] who reports an equilibrium separation for $ArH(A^2\Sigma^+)$ of 2.45 bohrs. In Table VI we have given the binding energy and equilibrium separation for the first three excited states of ArH. For comparison the results from the work of Olson and Liu[8] and Matcha and Milleur[7] have also been given. The absence of adequate polarization functions on H and the closed 3s subshell on Ar causes the MCVB to underestimate the dissociation energy and overestimate the equilibrium separation. We have tested the effect of opening the 3s shell by making a single calculation near the equilibrium separation. A 245 configuration calculation with open 3s subshell has a dissociation energy 0.15 eV greater than the closed calculation. We have not tested the effect of increasing the basis on H.

TABLE VI. Binding energy and equilibrium separation for $A^2\Sigma^+$, $B^2\Pi$, and $C^2\Sigma^+$ symmetry states.

State	Quantity	SCF[a]	MCVB[b]	SCF-CI[c]
$A^2\Sigma^+$				
	Re (bohr)	2.63	2.80	2.40
	De (eV)	2.250	2.436	3.856
$B^2\Pi$				
	Re	2.58	2.79	2.43
	De	1.892	1.890	3.041
$C^2\Sigma^+$				
	Re	2.60	2.79	2.39
	De	1.597	1.411	3.067

[a]Matcha and Milleur, Ref. 7.
[b]This work.
[c]Olson and Liu, Ref. 8.

Toennies and co-workers[17] have obtained an accurate potential for the ground state ($X^2\Sigma^+$) of ArH in the region (4.3 bohrs $\lesssim R \lesssim$ 9.1 bohrs). Measurements of the integral elastic cross sections for scattered hydrogen atoms have been analyzed and the experimental data fitted to a two parameter Lennard–Jones (6, 12) potential and a three parameter Slater–Buckingham exp(α, 6) potential. Results from our *ab initio* MCVB calculation are compared with the Lennard–Jones (6, 12) potential in Fig. 2.

III. RATE OF QUENCHING OF Ar ^3P BY H ATOMS

An examination of Fig. 1 shows that there is a somewhat isolated avoided crossing between the C and E curves at approximately 7 bohrs and another one between B and D at approximately 5 bohrs. If, during a collision, the diatomic system passes through these R values at an appropriate rate, then there is a high probability that the system will cross from one curve to another.

The Massey criterion[18] may be used to test this idea. The critical region between C and E has a $\Delta E \sim 0.13$ eV, $l \sim 1$ a.u., and $v = 1.2\times10^6$ cm/sec. This relatively high velocity is due, of course, to the acceleration

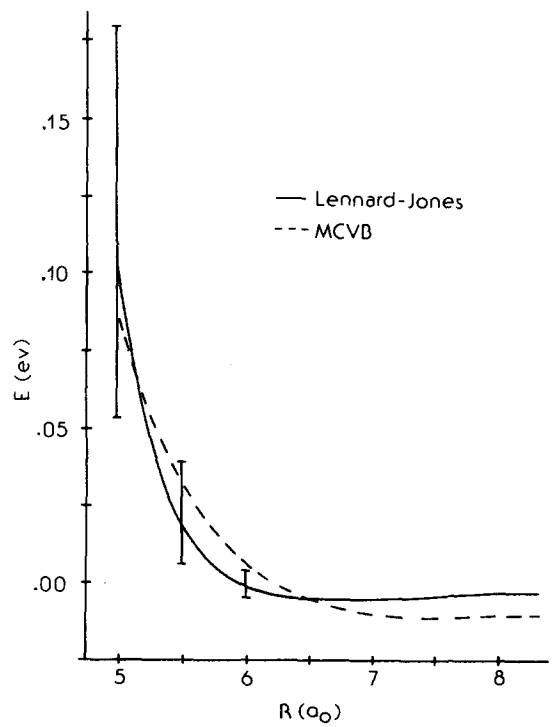

FIG. 2. Comparison of the *ab initio* ground state potential of ArH with the Lennard–Jones (6,12) potential given by Toennies *et al.* (Ref. 16).

TABLE VII. *Ab initio* parameters for the Landau–Zener model.

Parameter	$E\,^2\Sigma^+$, $C\,^2\Sigma^+$	$D\,^2\Pi$, $B\,^2\Pi$
$V_{12}(R)$ (eV)	0.065	0.159
ΔV (eV/bohr)	0.501	0.513
ΔE (eV)	0.768	1.154

produced by the fall of the E potential curve from its asymptotic level to the value near 7 bohrs. Combining these quantities we see that $\Delta El/\hbar v \sim 0.8$ which is neither very large nor very small. Although the Massey criterion is crude, it suggests that circumstances have cooperated in this system to give a reasonably high probability for curve switching under the conditions of the quenching experiments.

A more quantitative estimate of the rate constant is obtainable by use of Landau–Zener formula.[9] The probability for an electronic nonadiabatic transition between two molecular states is given as

$$P = 2e^{-w}(1 - e^{-w}) , \tag{5}$$

where w is given as

$$w = \frac{2\pi V_{12}}{\hbar\,|\Delta V'|\,v} .$$

The cross section for the process is given as

$$\sigma(v) = 2\pi \int_0^{b'} bP\,db , \tag{6}$$

where

$$b' = \left(R_c^2 + \frac{2\Delta E}{v^2} R_c\right)^{1/2}$$

and ΔE is the change in the reactant channel potential curve from its asymptotic value to its value at R_c, the internuclear separation at which the crossing takes place. The rate constant for the adiabatic transition can now be calculated by the introduction of the Boltzmann velocity distribution and integration over the entire velocity range.

We assume that the transfer of excitation from $Ar^*(n=4)$ to $H(n=2)$ proceeds via two different avoided crossings. One avoided crossing involves an interaction between the states $E\,^2\Sigma^+$ and $C\,^2\Sigma^+$ at $R = 6.61$ bohrs, while the second avoided crossing involves the states $D\,^2\Pi$ and $B\,^2\Pi$ at $R = 5.26$ bohrs. The rate constant for the proposed mechanism is given as

$$K = \tfrac{2}{3} k_\Pi + \tfrac{1}{3} k_\Sigma . \tag{7}$$

Parameters for the Landau–Zener model are given in Table VII and we calculate a rate constant of 25.2×10^{10} cm^3/sec.

IV. DISCUSSION

The description of experimental processes for excited states in terms of diabatic curves and their crossings can give a very useful picture of the physical effects operating. However, such curves are difficult to obtain from variational calculations, which, in practical cases, must give approximations to adiabatic states. Nevertheless, the MCVB wave functions are linear combinations of basis functions which correspond to well-defined asymptotic states, and an examination of the coefficients in the wave function can give insight concerning diabatic states.

When Ar and H are near the equilibrium position for R in the A state, the overlap between MCVB basis functions can be large, and several coefficients of wave function configurations can also be large due to near cancellations. At larger separations, the overlaps are considerably smaller. The significance of the coefficients in the MCVB wave function depends upon the purity of the corresponding basis functions. This can be tested by considering the inverse of the overlap matrix S^{-1}.[19] For the basis functions and corresponding coefficients we consider in the following analysis, the purity is never less than $0.3\ [=1/(S^{-1}_{ii})^{1/2}]$ at any interatomic distances greater than 5 a.u. This means that there are no cancellations possible beyond this level, and a given coefficient in the MCVB wavefunction is describing the amount of superposition of a unique attribute of its basis function. At longer distances the situation is even more favorable for this type of interpretation, of course, and we do not attempt to carry this analysis to small distances. When we examine the A, C, and E states specifically we find that in one or more of these the principal components of the wave function are the seven configurations listed in Table III.

In Figs. 3–5, we give the coefficients as a function of R for these configurations (where important) for each of the molecular states A, C, and E, and we refer to these for discussion.

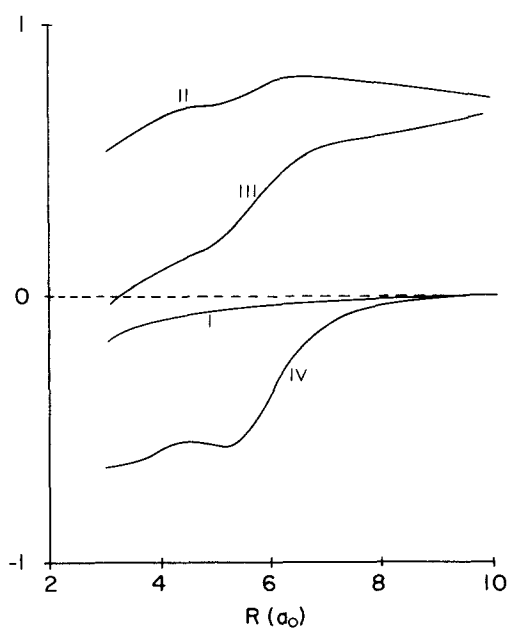

FIG. 3. Selected coefficients of the $A\,^2\Sigma^+$ molecular wave function as a function of R. Roman numerals indicate coefficients of similarily numbered molecular states in Table III.

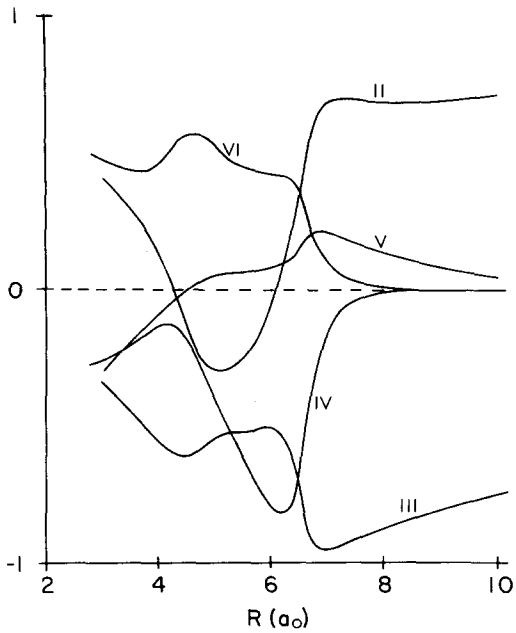

FIG. 4. Selected coefficients of the $C\,^2\Sigma^+$ molecular wave function as a function of R. Roman numerals indicate coefficients of similarily numbered molecular states in Table III.

A. *A* state

This state, which our calculations indicate to be largely uninvolved in the excitation exchange, is quite simple at long distances and is essentially a linear combination of II and III of equal admixture. We must mention that the H-atom basis in this calculation was oriented so that $(2s)+(2p_\sigma)$ is polarized away from the Ar atom. The very large polarizability of H in the $n=2$ state allows the electron to get away from the Ar effectively. The large dipole produced at the H end of the system also contributes to attraction at long distances by dipole-induced dipole interactions. The consequent polarization of Ar is not visible in any coefficients that can be seen at the scale in Fig. 3, of course. As R decreases, III is largely replaced by IV, the charge transfer state. This gives the A state at small distances the appearance of being a two-electron bond between Ar $3p_\sigma$ and H $1s$ "underneath" a hydridelike $1s'$ orbital. As can be seen, I is small at all distances.

B. *C* state

At large distances the C state is an admixture of II and III with the H($n=2$) state polarized strongly *toward* the Ar. As the internuclear distance decreases, there is a fairly sharp rearrangement of the states in the region of the 7 bohr C-E avoided crossing, with the charge transfer state IV and excited Ar state VI becoming important. At closer distances IV disappears and the H($n=2$) state changes to a polarization toward the Ar.

The presence of the V-type charge transfer state probably indicates a small coupling of state C to H Rydberg and continum states and may in part be due to deficiencies in our basis.

C. *E* state

In referring to Fig. 5 it is seen that the E state is a complex mixture of II–VII asymptotic states. At long distances, we have predominantly VI with a significant amount of VII. As the critical region is approached, the IV charge transfer state grows significantly, while VI and VII fall. Again at ~7 bohrs there is a relatively sharp switch to the states II and III with relative coefficients such that H($n=2$) is strongly polarized toward Ar. Farther in, the VI and VII states return strongly as II and III reduce in importance.

A close examination of C and E show that the sequence of events suggested by Setser is qualitatively substantiated by these calculations for the $^2\Sigma$ channels leading to exchange. In the present terms we have the system coming together in the E state, during which time the structure changes relatively slowly from $Ar(^3P)^*$–H to Ar^+–H^-. At the critical region near 7 bohrs, the velocity and energy curve separation induce a transition to the C state with reasonable probability and in so doing the structure remains largely as Ar^+–H^-. As the two atoms continue towards one another, complicated changes we do not consider take place. However, as the two atoms eventually separate the systems which remain on the C curve through the 7 bohr region convert from an Ar^+–H^- structure to Ar–H*($n=2$) which is the output channel we are interested in. Of course, a significant fraction of the system could execute the $E-C$ transition on the outward rather than the inward transit of the 7 bohrs region. The sequence of events and structures for these is qualitatively similar to those described above.

As we have seen above a significant number of the encounters undergo the transition in a $^2\Pi$ state. The states given in Table IV constitute the important components of B and D, and we give graphs of the coef-

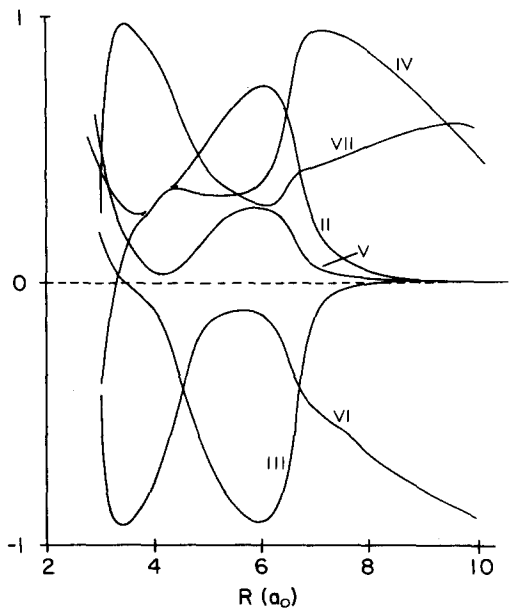

FIG. 5. Selected coefficients of the $E\,^2\Sigma^+$ molecular wave function as a function of R. Roman numerals indicate coefficients of similarily numbered molecular states in Table III.

ficients in Figs. 6 and 7.

We first see that these curves are rather featureless compared to the $^2\Sigma$ ones, even in the critical region near 5 bohrs.

D. *B* state

The *B* state is made up of only two states. At long distances I is the the only component, and by 5 bohrs III has become important. A covalent bond between Ar $3p_\sigma$ and H 1*s* has formed "underneath" the H $2p_\pi$ orbitals. This involves a charge transfer state in which H^- is predominately triplet 1*s*, $2p_z$. Such a state is certainly in the continuum for H^- alone, but in our system the presence of the Ar^+ nearby provides stabilization and makes it an important term in the *B* state, even at 5 bohr.

E. *D* state

At long distances, *D* is predominately VI and VII. As *R* decreases the normal charge transfer state II and the III increase slowly. In the critical region there is an increase in I which then falls off again. However, no great changes occur in any of the coefficients.

When considering the excitation exchange via the $^2\Pi$ channels we see that the charge transfer state plays a role somewhat different from that in the $^2\Sigma$ channels. As the atoms approach one another in the *D* state, the charge transfer effect grows slowly, but when the transition occurs there is some considerable rearrangement and the π-like character of the system jumps from Ar to H almost exclusively, still retaining the ionic character, however. As the atoms separate in the *B* state, the Ar pulls the H 1*s* back with it and leaves the H excited in the state which is the wanted exit channel for the reaction.

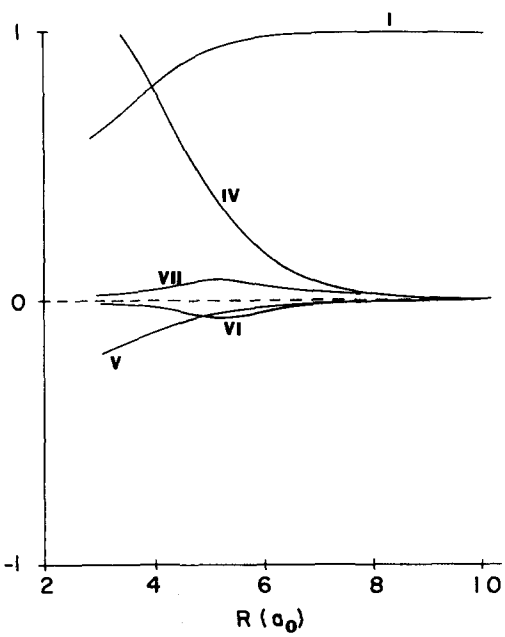

FIG. 6. Selected coefficients of the $B\,^2\Pi$ molecular wave function as a function of *R*. Roman numerals indicate coefficients of similarily numbered molecular states in Table IV.

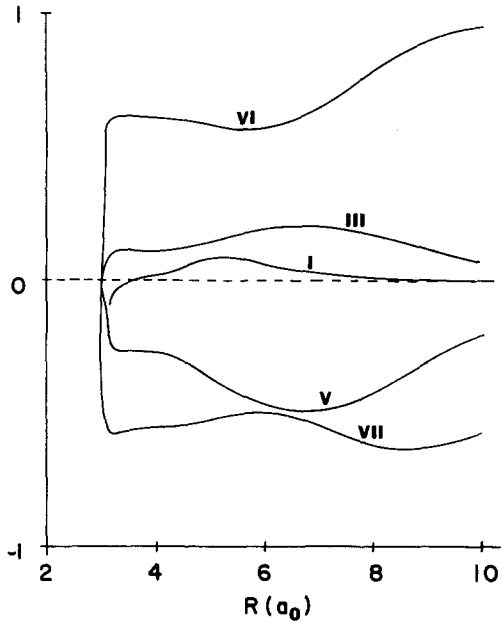

FIG. 7. Selected coefficients of the $D\,^2\Pi$ molecular wave function as a function of *R*. Roman numerals indicate coefficients of similarily numbered molecular states in Table IV.

V. CONCLUSIONS

We feel that the foregoing discussion gives a reasonable and convincing description of the processes leading to the quenching of $Ar(^3P)$ by H atoms. More complete CI calculations including additional configurations are not expected to modify the qualitative conclusions we have made from the present calculation.

Our calculated value of the rate constant is some ten times too large, but this reflects the special features of this system which cooperate to produce this large rate constant. In addition, all our qualitative estimates of curve switching rates have used two-state models. In a region with as many curves as this, there are other outgoing channels leading to other products and perhaps returning to the reactants, all of which we have ignored. All of these are expected to reduce the calculated rate constant.

ACKNOWLEDGMENTS

The authors wish to express their sincere appreciation to the National Science Foundation for the support of this work through CHE76-17567. We wish to thank Professor D. W. Setser for useful discussions on this problem, and we wish to thank Dr. R. Olsen and Dr. B. Liu for sending their calculations before the publication. Finally, we wish to thank the Computing Network of the University of Nebraska for the computing time necessary to make this study.

[1] J. W. C. Johns, J. Mol. Spectrosc. 36, 488 (1970).
[2] V. E. Bondybey, G. C. Pimentel, and P. N. Noble, J. Chem. Phys. 55, 540 (1971).
[3] V. E. Bondybey and G. C. Pimentel, J. Chem. Phys. 56, 3832 (1972).
[4] V. E. Bondybey, P. K. Pearson, and H. F. Schaefer III, J. Chem. Phys. 57, 1123 (1972).

[5]M. A. A. Clyne, P. B. Monkhouse, and D. W. Setser, Chem. Phys. 28, 447 (1978).
[6]R. E. Olson and B. Liu, Phys. Rev. A 17, 1568 (1978); A. F. Wagner, G. Das, and A. C. Wahl, J. Chem. Phys. 60, 1885 (1974).
[7]R. L. Matcha and M. B. Milleur, J. Chem. Phys. 69, 3019 (1978).
[8]R. E. Olson and B. Liu (unpublished results).
[9]L. D. Landau, Phys. Z. Sowjetunion 2, 46 (1932); C. Zener, Proc. R. Soc. A 137, 696 (1932); J. Heinrichs, Phys. Rev. 176, 141 (1968).
[10]G. A. Gallup, Int. J. Quantum Chem. 6, 761, 899 (1972); G. A. Gallup, Adv. Quantum Chem. 7, 113 (1973).
[11]J. L. Whitten, J. Chem. Phys. 39, 349 (1963).
[12]J. D. Petke, J. L. Whitten, and A. W. Douglas, J. Chem. Phys. 51, 256 (1969).
[13]S. J. Sramek and G. A. Gallup (unpublished results).
[14]G. A. Gallup, Mol. Phys. 33, 943 (1977).
[15]R. L. Vance and G. A. Gallup (manuscript in preparation).
[16]R. Klingbeil, J. Chem. Phys. 57, 1066 (1972).
[17]R. W. Bickes Jr., B. Lantzsch, J. P. Toennies, and K. Walaschewski, Faraday Discuss. Chem. Soc. 55, 67 (1973).
[18]J. B. Hasted and A. R. Lee, Proc. Phys. Soc. London 79, 702 (1962).
[19]G. A. Gallup and J. M. Norbeck, Chem. Phys. Lett. 21, 495 (1973).
[20]C. E. Moore, *Atomic Energy Levels*, National Bureau of Standards Circular No. 467 (U. S. GPO, Washington, D. C., 19xx).